Atorvastatin suppresses HIV/antiretroviral drug-induced cardiac fibrosis and dysfunction in mice by blocking platelet TGFβ1 signaling

Kumar Subramani[a], Denys Babii[a], Brienne Cole[a], Tayyab A. Afzal[a], Thamizhiniyan Venkatesan[a], Trevor Word[a], Sandra Gostynska[a], Sixia Chen[a,b], Kar-Ming Fung[a,b], Ali Danesh[c], Itzayana G. Miller[c], Paul Klotman[d], Brad R. Jones[c], Jeffrey Laurence[e], and Jasimuddin Ahamed[a,b,1]

[a]Cardiovascular Biology Research Program, Oklahoma Medical Research Foundation, Oklahoma City, OK 73104; [b]University of Oklahoma Health Sciences Center, Oklahoma City, OK 73104; [c]Division of Infectious Diseases, Weill Cornell Medical College, New York, NY 10065; [d]Baylor College of Medicine, Houston, TX 77030; and [e]Division of Hematology and Medical Oncology, Weill Cornell Medical College, New York, NY 10065.

Running Title: Role of platelet TGFβ1 in organ fibrosis

[1]To whom correspondence may be addressed. Jasimuddin Ahamed, Ph.D. Email**:** ahamedj@omrf.org.

Author Contributions: JA, JL, KS, DB, TW, BRJ, PK, and BC designed the research protocol; KS, DB, TW, BC, TAA, TV, SG, AD, and IGM performed the research; KS, DB, TW, KMF and SC analyzed the data; JA and JL acquired funding; JA and JL wrote the paper with clinical conceptualization.

Competing Interest Statement: The authors declare no competing interests.

Data Sharing: For original data, please contact the corresponding Author's lab.

Keywords: antiretroviral therapy, HIV, cardiac fibrosis, platelets, transforming growth factor-β1

Main Text 4470
Figures 1 to 7
Tables: 1

Key Points:

- Contemporary ART regimens induce the release of platelet TGFβ1 and are associated with cardiac fibrosis, diastolic dysfunction, and ectopic fat deposition in HIV-infected mice.
- Depletion of platelet TGFβ1 and/or atorvastatin therapy suppresses HIV-ART-induced cardiac fibrosis, suggesting anti-platelets and statins may be useful to prevent heart failure among PWH.

Abstract

Cardiovascular disease (CVD), both atherosclerosis-related and heart failure with preserved ejection fraction (HFpEF) linked to cardiac fibrosis, contributes to morbidity and mortality in people with HIV (PWH) receiving antiretroviral therapy (ART). In the REPRIEVE trial, pitavastatin reduces atherosclerotic CVD risk to a magnitude inconsistent with pitavastatin's impact solely on LDL-cholesterol and inflammation. We hypothesized that HFpEF in PWH is related to HIV-induced fibrosis mediated by platelet TGFβ1, is accelerated by certain contemporary ART, and may also be inhibited by statins. ART drugs used in REPRIEVE, including a nucleoside/nucleotide, integrase inhibitor-based regimen (tenofovir (TDF), emtricitabine (FTC), and dolutegravir (DTG)), and the protease inhibitors ritonavir (RTV) and darunavir (DRV), and the impact of atorvastatin, were examined in two HIV mouse models: transgenic HIV-Tg26 mice and HIV-PDX mice engrafted with T cells isolated from PWH. HIV-Tg26 and HIV-PDX mice had higher cardiac fibrosis than littermate controls without HIV ($p<0.05$). Administration of TDF-FTC-DTG or RTV, but not DRV, resulted in a further ~2-fold increase in fibrosis ($p<0.01$). Cardiac fibrosis and intracardiac fat accumulation correlated with reduced diastolic function. Mice depleted of platelet TGFβ1 (TGFβ1$^{Platelet\text{-}\Delta}$Tg26*)*, or treated with atorvastatin, were partially protected from HIV- and ART-induced cardiac fibrosis, steatosis, and diastolic dysfunction. Atorvastatin effects were independent of changes in inflammatory cytokines. These effects correlated with reduced platelet activation and TGFβ signaling in cardiac endothelial cells, fibroblasts, and macrophages undergoing mesenchymal transition. Our results indicate that certain ART regimens accelerate HIV-associated CVD characterized by HFpEF via platelet TGFβ1-dependent processes, which were mitigated by atorvastatin. We postulate that our findings provide a potential mechanism for the pleiotropic effects of statins in HIV/ART-linked CVD which could be targeted by antiplatelet agents or inhibition of TGFβ signaling.

Introduction

HIV infection has been linked to several non-AIDS-defining illnesses, particularly cardiovascular disease (CVD). This contributes significantly to morbidity and mortality in people with HIV (PWH) despite effective antiretroviral therapy (ART) (1). A major advance in terms of prevention derives from the Randomized Trial to Prevent Vascular Events in HIV (REPRIEVE), demonstrating that pitavastatin decreased atherosclerotic CVD among ART-treated PWH (2). The observed reduction was much greater than predicted based on the magnitude of decrease in LDL-cholesterol achieved (2). In terms of potential mechanisms, pitavastatin had no effect on other non-AIDS-defining comorbidities which, like atherosclerotic CVD, have been linked to chronic inflammation among ART-treated PWH, including end-stage liver disease, end-stage renal disease, tuberculosis, and malignancy (2, 3). Indeed, while a decrease in lipoprotein-associated phospholipase A2, a marker of arterial inflammation, was reported among REPRIEVE participants receiving pitavastatin, there was no change in other pro-inflammatory biomarkers, including hsCRP, MCP-1, sCD14, CD163, IL-1β, IL-6, IL-10, IL-18, and caspase-1 (3).

A recent secondary analysis of REPRIEVE found that pitavastatin increased procollagen C-endopeptidase enhancer 1 (PCOLCE), which enhances activity of proteinases essential for the formation and assembly of vascular extracellular matrix (4). Those processes may be associated with the transformation of vulnerable plaque phenotypes to more stable coronary lesions (4), consistent with the impact of pitavastatin on early atherosclerotic cardiovascular events in that trial. This is similar to the protective effects of the pro-fibrotic cytokine TGFβ1 in early atherosclerosis, which promotes collagen synthesis and plaque stability, although the opposite effects have been suggested in later stages of atherosclerosis, with plasma TGFβ1 levels significantly increased in patients with coronary artery ectasia and coronary artery disease (5). However, emerging data related to HIV-linked CVD in general, and the heart failure mechanisms and phenotypes that predominate among PWH in the contemporary ART era, have the potential to further modify CVD treatment and prevention strategies (6). With this concern, we sought preclinical evidence on the ability of statins to influence heart failure with preserved ejection fraction (HFpEF), which is characterized by myocardial fibrosis and steatosis in both PWH and the general population (7-11). It is now recognized in 35% of CVD cases in PWH on ART (6).

Disentangling the effects of HIV versus ART on myocardial structural and functional pathology through patient-oriented research is challenging, given the potential divergent effects of different ART drugs and drug classes (12-15). In our study, we leveraged two established mouse models of HIV: (i) transgenic Tg26 mice expressing seven HIV proteins but producing no infectious virus (HIV-Tg26) (16); and (ii) HIV patient-derived xenograft (HIV-PDX) mice, which are nonobese diabetic severe combined immunodeficiency IL2rγ^{null} mice engrafted with HIV-infected memory CD4+ T-cells from PWH (17). We exposed these mice to ART drugs used in REPRIEVE, including a nucleoside/nucleotide and integrase strand transfer inhibitor (INSTI)-based regimen as well as protease inhibitors (PI) used in PI-boosted regimens. Both INSTI- and PI-based ART are associated with an increased risk of many forms of CVD compared with non-nucleoside reverse transcriptase inhibitor-based ART (13-15, 18-21). We characterized myocardial structural and functional pathology at eight weeks post-treatment. We also tested whether atorvastatin, a lipophilic statin in the same class as pitavastatin, could protect cardiac structure/function in the same settings, and explored the mechanisms underlying such preservation. These data suggest a novel potential pathway by which

statins influence specific forms of CVD in ART-treated PWH. This mechanism appears to operate independently of changes in total cholesterol and inflammatory cytokines, aligning with observations from the REPRIEVE trial.

Results

HIV-Tg26 and HIV-PDX Mice Have Higher Cardiac Fibrosis Than Littermate Controls Without HIV. An INSTI-based ART Regimen and the PI RTV Further Increased Cardiac Fibrosis. We previously showed that wild-type (wt) C57Bl/6 mice treated with supra-therapeutic doses of ritonavir (RTV) had an approximately three-fold increase in cardiac fibrosis compared to untreated mice (~1.5% vs. ~0.5%) (22). Since PWH treated with PI-based ART appear at greatest risk for CVD (14, 15), including cardiac fibrosis, we first tested whether HIV alone is associated with enhanced cardiac fibrosis in mice, and then whether doses of RTV equivalent to that used clinically in RTV-boosted PI regimens, or a common, INST-based ART regimen, tenofovir (TDF), emtricitabine (FTC), and dolutegravir (DTG), enhance such fibrosis. Only 2 of 10 (20%) wt littermate control mice on an FVB/NJ, C57Bl/6 or NSG background had mild cardiac fibrosis (~1.5% of the total cardiac area) at 4 months of age, as measured by Masson trichome and picrosirius red staining. In contrast, 8 of 11 (73%) of HIV-Tg26 mice--those containing 7 HIV-1 genes but incapable of producing infectious virus--developed mild to moderate fibrosis (2-4% of the total cardiac area). Administration of RTV or TDF-FTC-DTG, i.p. daily for eight weeks, led to moderate cardiac fibrosis (3-4% of the total cardiac area) in 12 of 15 (80%) of these mice. ($P = 0.003$ for wt control vs. HIV-Tg26 mice and $P = 0.007$ for HIV-Tg26 vs. RTV-treated HIV-Tg26 mice) (**Fig.1A, B, and 1D;** Fig. S2).

As a control, we challenged HIV-Tg26 (**Fig. 1A, B, and 1D**) and wt C57Bl/6 (Fig. S2) mice with clinically relevant doses of darunavir (DRV) alone. This PI has not been linked clinically to CVD in the absence of RTV boosting (14). We found no elevation of cardiac fibrosis over pre-treatment levels in either HIV-Tg26 or wt mice. Hematologic values (including RBC, WBC, and platelet count) showed that Tg26 mice were mildly anemic and thrombocytopenic, but all other parameters were similar to those observed in control mice (**Table 1**). Platelet aggregation responses induced by ADP or thrombin were also similar in platelets isolated from Tg26 and control mice (data not shown).

Comparable results were observed in HIV-PDX mice infected with HIV with and without TDF-FTC-DTG treatment (**Fig.1C-E**). Nine of 11 (82%) mice exhibited both perivascular and interstitial fibrosis with TDF-FTC-DTG treatment compared with 40% of HIV-PDX mice not exposed to these drugs, as assessed by Masson trichome and picrosirius red staining and imaging under normal- and-polarized light, respectively (**Fig.1C-E**).

Both an INSTI-based ART Regimen and RTV Induce Diastolic Dysfunction with Preserved Ejection Fraction in HIV Mice. To assess whether the degree of fibrosis seen in ART-treated HIV mice was of functional significance, we evaluated cardiac function by echocardiography. Systolic dysfunction was not observed based upon preservation of both ejection fraction (EF) and fractional shortening (FS), in wt and TDF-FTC-DTG-treated HIV-Tg26 mice (Fig. S3). Diastolic function in HIV-Tg26 mice was slightly impaired compared with HIV negative wt controls in the absence of ART ($p=0.03$). More severe diastolic dysfunction was noted in both INSTI- and RTV-challenged HIV-Tg26 mice, compared with non-drug treated HIV-Tg26 mice, manifested as higher early-to-late (E/A) ventricular filling velocity ratios (**Fig. 2A-C**; $p<0.01$). There was a significant correlation between cardiac fibrosis and

diastolic indices, specifically E/A ratios, in HIV-Tg26 mice with and without ART compared with control Tg26 mice (**Fig. 2D**).

In terms of potential mechanisms, we previously showed that RTV induces release of TGFβ1 *in vitro* from human platelets (21). We now show that RTV alone, as well as the TDF-FTC-DTG cocktail, induce release of TGFβ1 from freshly isolated human platelets whereas the PI DRV had no effect (**Fig. 2E**). RTV and TDF-FTC-DTG also induced release of TGFβ1 *in vivo* as assessed in plasma from ART-treated HIV-Tg26 mice (**Fig. 2F**).

ART-Induced Ectopic Fat Deposition in the Heart is Associated with Cardiac Fibrosis in HIV Mice. Cardiac fat deposition is increased in ART-treated PWH and is associated with diastolic dysfunction (18, 19). However, its relationship to cardiac fibrosis in the setting of HIV/ART has not been examined. We evaluated the effect of RTV and TDF-FTC-DTG on fat accumulation in hearts of HIV-Tg26 and HIV-PDX mice. Both ART regimens resulted in higher cardiac fat deposition, as shown by Oil-Red O staining (Fig. 3A-B). To determine whether these stained areas contained fat cells, they were immunostained with an antibody to perilipin, a marker of fat cells, which revealed clusters of perilipin-positive fat cells (**Fig. 3A, B**).

The same heart sections were then stained with picrosirius red, Masson trichome, and H&E. Fibrotic areas with excessive collagen accumulation surrounded by fat cells were recognized in superimposed images (**Fig. 3A**, bottom panels). Quantification confirmed the association between fibrosis and lipid/fat cell accumulation in ART-treated hearts of both HIV-Tg26 and HIV-PDX mice (**Fig. 3C**). Taken together, these results indicate that ART-treated HIV mice with higher cardiac fibrosis also have greater cardiac fat cell deposition.

Platelet-derived TGFβ1 Contributes to RTV-induced Cardiac Fibrosis and Fat Cell Deposition. We previously showed that platelet TGFβ1 contributes to RTV-induced cardiac fibrosis in wt C57Bl/6 mice (22). To test whether platelet TGFβ1 contributes to cardiac fibrosis in mice treated with various ART drugs in the context of HIV, we generated HIV-Tg26 mice with platelet TGFβ1-deficient (TGFβ1$^{Platelet-\Delta}$Tg26) by crossing HIV-Tg26 mice with PF4CreTgfb1$^{flox/flox}$ mice. We found a >90% decrease in total TGFβ1 in platelets and serum, and a 50% decrease in plasma of TGFβ1$^{Platelet-\Delta}$Tg26 mice compared to littermate control HIV-Tg26 mice (**Fig. 4A**). This indicates that platelets are the major source of circulating TGFβ1 in HIV mice. However, although, platelets are the most abundant source of TGFβ1, other cells, including macrophages, dendritic cells, regulatory T cells, and B cells could also produce TGFβ1 (23).

We observed reduced levels of cardiac fibrosis in RTV-treated TGFβ1$^{Platelet-\Delta}$Tg26 mice (2.1% ± 0.25%) compared with RTV-treated HIV-Tg26 littermate mice (4.68% ± 0.85%; P <0.01) (**Fig. 4B**). The percentage of areas of fibrosis was 2.1% ± 0.25% in TGFβ1$^{Platelet-\Delta}$Tg26 mice vs. 4.68% ± 0.85% in HIV-Tg26 mice (P <0.01). Reduced fibrosis in RTV-treated TGFβ1$^{Platelet-\Delta}$Tg26 mice was accompanied by protection from diastolic dysfunction (**Fig. 4C**). Since ART-induced accumulation of lipid/fat cells in the heart correlated with fibrosis, we also assessed lipid/fat cell accumulation in TGFβ1$^{Platelet-\Delta}$Tg26 mice. Staining of RTV-treated TGFβ1$^{Platelet-\Delta}$Tg26 mouse hearts with Oil-Red O revealed lower lipid accumulation compared to HIV-Tg26 littermates challenged with RTV. Immunostaining with perilipin confirmed less accumulation of fat cells in these mice compared to littermate controls (**Fig. 4D, E**). The presence of fat cells correlated with levels of fibrosis in TGFβ1$^{Platelet-\Delta}$Tg26 and HIV-Tg26 littermate control mice challenged with RTV (**Fig. 4F**).

To test whether ART-associated release of TGFβ1 *in vivo* is likely to be primarily derived from platelets, we challenged TGFβ1$^{Platelet-\Delta}$Tg26 mice with RTV and TDF-FTC-DTG. No increase in TGFβ1 levels over baseline was observed (data not shown), indicating that ART increases TGFβ1 *in vivo* primarily by activating platelets.

Atorvastatin Suppresses TGFβ Signaling, Cardiac Fibrosis and Fat Accumulation, and Diastolic Dysfunction Without Altering Inflammatory Cytokines and Total Cholesterol in HIV Mice. The REPRIEVE trial showed that pitavastatin, a lipophilic statin, had a beneficial effect in reducing atherosclerotic CVD (2). We first tested whether another lipophilic statin, atorvastatin, could influence processes related to the second major type of CVD linked clinically to HIV/ART, fibrosis-associated HFpEF, by inhibiting TGFβ1-induced signaling. We used an engineered cell culture system in which TGFβ1 stimulation induces PAI1 luciferase activity in mink lung epithelial cells (MLEC) expressing a TGFβ-responsive PAI1 reporter fused with a luciferase gene (24). This signaling response was inhibited by atorvastatin in a dose-dependent manner (**Fig. 5A**). This is consistent with the finding that TGFβ1-induced SMAD2/3 phosphorylation signaling was inhibited by atorvastatin, also in a dose-dependent manner (**Fig. 5B-C**). Atorvastatin also inhibited TGFβ1-induced signaling responses assessed by PAI1 and SMAD phosphorylation *in vitro* in the presence of RTV or TDF-FTC-DTG (Fig. S5A-C).

To investigate whether atorvastatin could prevent HIV-linked cardiac fibrosis in HIV mice *in vivo*, we administered 3 mg/kg in drinking water to HIV-Tg26 mice and measured cardiac fibrosis and heart function. This dose corresponds to 20 mg/day in an 80-kg human and is well-tolerated in mice, without toxicity (25, 26). Less cardiac fibrosis and impairment of diastolic function was observed compared to untreated HIV-Tg26 mice over an eight-week period (**Fig-5D-E**). Atorvastatin administration along with TDF-FTC-DTG or RTV to HIV-Tg26 mice also reduced cardiac fibrosis and preserved diastolic function compared to ART-exposed HIV-Tg26 mice not receiving atorvastatin (**Fig. 5D-F;** Fig. S6). Treatment of TGFβ1$^{Platelet-\Delta}$Tg26 mice with atorvastatin did not further deteriorate diastolic function compared to basal levels (**Fig. 5G**), with no change in cardiac fibrosis levels (2.0% ± 0.2% in TGFβ1$^{Platelet-\Delta}$Tg26 mice vs. 2.1% ± 0.5% in ATV-treated mice), indicating ATV inhibits cardiac fibrosis and diastolic dysfunction by blocking platelet-TGFβ1-induced signaling.

Atorvastatin did not alter inflammatory cytokines IL-6 and TNF-α, PPAR-gamma or plasma total cholesterol and glucose levels in HIV-Tg26 mice with or without ART treatment (Fig. S4; Fig. S9). Staining of heart sections with Masson trichome, Picrosirius-red, or Oil-Red O and perilipin revealed lower fibrosis and lipid/fat cell accumulation in atorvastatin-treated vs. vehicle treated mice challenged with TDF-FTC-DTG or RTV (Fig. S6). Collectively, these results indicated that atorvastatin inhibits cardiac fibrosis and diastolic dysfunction by blocking platelet-TGFβ1-induced signaling.

Atorvastatin Inhibits Platelet Activation and TGFβ Signaling and Suppresses Myofibroblast Transition and Collagen Expression in Cardiac Cells. Atorvastatin inhibits platelet activation induced by classic platelet agonists (27). We now show that it inhibited human platelet activation *in vitro* as well as reduced plasma TGFβ1 levels in mice co-treated with certain antiretroviral drugs (Fig. S7).

To test whether atorvastatin blocks TGFβ signaling *in vivo*, we performed multicolor immunofluorescence and confocal microscopy on HIV-Tg26 mouse hearts with and without atorvastatin treatment, and in mice deficient in platelet TGFβ1 (TGFβ1$^{Platelet-\Delta}$Tg26). HIV-Tg26 mice had higher TGFβ signaling, as revealed by of SMAD2 and SMAD3

(pSMAD2/3) phosphorylation in cells within areas of perivascular fibrosis (**Fig. 6** and Fig. S8). Cells positive for pSMAD3 were also positive for αSMA and/or collagen, or periostin (**Fig. 6A** and Fig. S8), indicating that they were undergoing mesenchymal transition to myofibroblasts. Myofibroblasts produce excessive collagen in tissues undergoing pathologic fibrosis (**Fig. 7**) (28). HIV-Tg26 mice treated with atorvastatin had significantly lower levels of nuclear pSMAD2/3 translocation in cells co-expressing myofibroblast markers (**Fig. 6** and Fig. S8), suggesting that atorvastatin inhibits TGFβ1-induced signaling linked to fibrosis-related gene responses *in vivo*.

To identify additional cells contributing to mesenchymal transition, producing excessive collagen via induction of TGFβ1 signaling and fibrosis, we co-stained heart sections with fibroblast (PDGFβR)-, endothelial cell (CD31)-, and macrophage (CD206)-specific markers. RTV- or TDF-FTC-DTG-treated HIV-Tg26 mice had more cells co-expressing these markers along with α-SMA, collagen, periostin, and pSMAD3. In comparison, atorvastatin-treated HIV-Tg26 mice showed fewer cells with such colocalized signals and had significantly lower nuclear pSMAD2/3 translocation (**Fig. 6A**–**C** and Fig. S8). This suggests that atorvastatin inhibits TGFβ1-induced fibrotic gene responses *in vivo*. Correspondingly, collagen-positive areas reflecting myofibroblast transition were lower in atorvastatin-treated HIV-Tg26 hearts compared with their vehicle-treated counterparts (**Fig. 6**). Additionally, TGFβ1-induced expression of myofibroblast marker genes alpha-smooth muscle actin (*ACTA2*) and collagen type 1 alpha 1 (*COL1A1)* were blocked in atorvastatin-treated HIV-Tg26 mice (Fig. S5D).

Taken together, these data indicate that platelet-derived TGFβ1-mediated signaling in cardiac cells, including endothelial cells, fibroblasts, and macrophages, can trigger their transformation into excessive collagen-producing myofibroblasts, inducing cardiac fibrosis. These processes can be mitigated by atorvastatin or by inhibiting or depleting platelet TGFβ1 (**Fig. 7)**.

Discussion

Our work investigating HIV/ART-induced cardiac pathology in mouse models of HIV infection yielded several findings of clinical relevance to accelerated heart failure with preserved ejection fraction (HFpEF) seen in PWH, providing insights into potential mechanisms. We previously showed that platelet-derived TGFβ1 is an important mediator of RTV-associated cardiac fibrosis in wt mice (22). We now show that a lower dose of RTV, as used in PI-boosted ART regimens, but not the PI DRV alone, and the INSTI-based regimen TDF-FTC-DTG, augment cardiac fibrosis and diastolic dysfunction in the context of HIV, above levels seen with HIV alone. The level of cardiac fibrosis in HIV/ART mice, 3-4%, was equivalent to that estimated by imaging studies in ART-treated PWH (2-3%) (29) and sufficient to induce diastolic dysfunction. It was accompanied by cardiac steatosis, also a feature of HFpEF in ART-treated PWH. Areas of ART-induced fibrosis in HIV/ART mice were accompanied by myofibroblast infiltration with elevated levels of SMAD2/3 phosphorylation, reflecting TGFβ1 signaling and excess collagen production. A role for platelet TGFβ1 in cardiac fibrosis associated with certain ART drugs was further supported by the correlation of plasma TGFβ1 with both fibrosis and diastolic dysfunction.

In terms of practical interventions, atorvastatin protected HIV-Tg26 mice, both untreated and exposed to either RTV or the INSTI-based cocktail TDF-FTC-DTG, from cardiac fibrosis and steatosis and diastolic dysfunction. These effects appear to be channeled, at least in part, through the inhibition of TGFβ signaling. They correlated with the presence of fewer myofibroblasts in the hearts of HIV/ART mice treated with

atorvastatin vs. vehicle. Our results are consistent with the known antioxidant/anti-inflammatory effects of statins (30), and with atorvastatin's ability to attenuate the rise in soluble ST2, a marker of fibrosis in PWH on ART (31). Although pitavastatin has a relatively stronger effect on HDL-cholesterol than atorvastatin (32), the latter has other salutary effects. It can significantly reduce non-calcified coronary plaque volume relative to placebo in PWH on ART, despite no change in HDL-cholesterol (33). It also has an indirect immunomodulatory effect in the setting of HIV, increasing Treg and inhibiting expression of the critical HIV coreceptor CCR5 (34). Finally, although potential drug-drug interactions with statins and ART are primarily based on theoretical considerations, caution is recommended using atorvastatin, but not pitavastatin, in the setting of PI-based ART, due to its effects on cytochrome CYP3A4 (35). However, NRTIs and INSTIs share an affinity for the BCRP (breast cancer resistance protein) drug transporter with pitavastatin, while no such interaction has been observed with atorvastatin (35). The choice of a specific statin for CVD prophylaxis in PWH on ART may need to be individualized based on these and other more traditional CVD risk considerations.

Our observations dovetail with recent work by Marunouchi et al. demonstrating that statins suppressed cardiac fibrosis and diastolic dysfunction in wt mice fed a high-fat diet and exposed to the nitric oxide synthetase inhibitor N[w]-nitro-L-arginine methyl ester hydrochloride as a chemical means of inducing HFpEF (36). Assessment of cardiomyocytes from statin pre-treated vs. control mice also revealed decreased phosphorylation of SMAD and MAPK, enzymes downstream of TGFβ, reflecting reduced TGFβ signaling in those cells (36). Our in vitro data showing that atorvastatin dose-dependently inhibits TGFβ1-induced SMAD2/3 signaling and TGFβ-responsive profibrotic responses, including PAI-1 and α-SMA, are also consistent with studies in human cardiac fibroblasts demonstrating that atorvastatin suppresses SMAD and MAPK signaling (37). Our data further extend previous studies (27) indicating that atorvastatin can block platelet activation linked to standard agonists (ADP, collagen, and arachidonate) as well as certain cytokines. In our study, PPAR-gamma, known to be affected by atorvastatin, albeit via an unknown mechanism, remained unchanged across groups and treatments (Fig. S9). It is thus plausible that statins act via a dual mechanism in HIV/ART-associated CVD characterized by HFpEF, blocking TGFβ1 release from platelets and subsequently inhibiting TGFβ signaling in cardiac cells.

In terms of the impact of atorvastatin on cholesterol and inflammation, two traditional risk factors for CVD, statins can lower inflammatory cytokines and LDL-cholesterol in humans, but these effects did not correlate with the ability of a related lipophilic statin, pitavastatin, to impact atherosclerotic CVD in PWH on ART (2). Those results are paralleled by our mouse models, which showed no significant reduction in IL-6, TNF-α, or total cholesterol. We acknowledge that our data are not conclusive regarding whether atorvastatin's effects are completely independent of the modulation of cholesterol metabolism.

Our focus on TGFβ and fibrosis should also be viewed in the general context of HIV/ART-linked CVD risk, both atherosclerotic and fibrosis-associated. In REPRIEVE, pitavastatin increased the abundance of PCOLCE, which enhances proteinases involved in vascular extracellular matrix production, favoring the transformation of plaques that are vulnerable to fragmentation to more stable coronary lesions (4). This is consistent with the salutary effects of TGFβ1 in the early stages of atherosclerosis (5). In later stages, when pathologic fibrosis and HFpEF develop, suppression of TGFβ signaling may be beneficial. Both early and late stages of CVD in PWH might therefore benefit from statin intervention, albeit for distinct reasons. Although there are no validated tools to predict who among

PWH receiving ART may clinically progress to HFpEF, the newly developed American Heart Association PREVENT HF risk score has proven valuable in a limited clinical study of such individuals (38).

The concomitant development of cardiac steatosis and fibrosis in our ART-treated HIV mice is also of interest. Among PWH in REPRIEVE, increased peri-coronary adipose tissue density was independently associated with the prevalence and severity of coronary plaque (39). However, the interplay between pathways leading to cardiac fibrotic and steatosis is incompletely understood. While ART-treated PWH without heart failure have higher levels of cardiac fibrosis and steatosis compared with individuals without HIV, cardiac steatosis stands out as the structural pathology correlating most closely with diastolic dysfunction (10, 29, 40, 41). Cardiac magnetic resonance spectroscopy studies reveal excess intramyocardial lipid deposition among ART-treated PWH in association with reduced diastolic function (10, 40). Certain ART drugs are also associated with ectopic visceral and hepatic fat deposition (42). Our findings underscore the need for further exploration of HIV/ART-induced cardiac fat accumulation. Cardiac steatosis is an emerging global problem among ART-treated PWH (1, 19), paralleling rising rates of obesity in this population (43). Future studies could assess whether anti-obesity therapeutics known to confer cardioprotection, such as glucagon-like peptide 1 receptor agonists (GLP-1 RA) (44), reduce cardiac and other ectopic fat accumulation in PWH. In this regard, a pilot study of ART-treated PWH receiving the GLP-1 RA semaglutide revealed weight loss accompanied by a significant reduction in liver fat (45).

Our study has limitations. Based on our prior work with RTV, we focused our mechanistic experiments on TGFβ pathways leading to fibrosis. However, other pathways may also be relevant. In terms of the impact of HIV and ART on diastolic vs. systolic function and links to fibrosis, we did find a small decrease in EF in HIV-Tg26 vs. wt mice. But no further decrease occurred after ART treatment, and those EF values were still within the normal range for systolic heart function. However, our studies were terminated at 8 weeks; ART influence on EF might require longer periods, a subject for future investigation. Our work was strengthened by studying ART-induced cardiac pathology in two different mouse models of HIV, as well interrogation of ART's effects in mice with platelet-specific TGFβ1 deletion to gain mechanistic insights. We also explored the impact of concomitant statin therapy, paving the way for clinical correlations. Selection among classes of ART drugs, and individual drugs within classes, based on data presented here, could be considered. Apart from statins, suppression of ART-induced TGFβ1 release from platelets and its activation could be explored. This might be accomplished via anti-platelet agents, compounds that inhibit TGFβ1 release from platelets, and pharmacological inhibition of TGFβ signaling, such as with galunisertib (46).

Methods

Sex as a biological variable.

Mouse Experiments. Each mouse was numbered, and all experiments were performed by investigators blinded to mouse genotype. All mice used (aged 6–10 weeks of old) were housed in a controlled environment (23°C ± 2°C; 12-h light/dark cycles) and fed a standard diet (PicoLab Rodent Diet). Both male and female mice were included in this study to account for sex as a biological variable. HIV-Tg26 is a transgenic mouse expressing seven of the nine HIV proteins under the control of a viral LTR promoter (16). They were

bred with either FVB/NJ mice or C57Bl/6 background for at least 10 generations. To create a platelet-specific knockout of the *Tgfb1* gene on a Tg26 background, we crossed PF4CreTgfb1$^{flox/flox}$ *(*TGFβ1$^{Platelet-\Delta}$*)* mice (28) with HIV-Tg26 mice to generate TGFβ1$^{Platelet-\Delta}$Tg26 mice*.* We confirmed the inactivation of the *Tgfb1*-floxed allele in platelets by genotyping and performed phenotypic characterization by measuring TGFβ1 levels in platelets, serum, and plasma of mice homozygous for TGFβ1$^{Platelet-\Delta}$Tg26. Tg26 littermates without Gp1bCre or Tgfb1$^{flox/flox}$ were used as controls.

All mice infected with replication-competent HIV were housed in the animal facility of the Belfer Research Building at Weill Cornell Medicine. Humanized HIV-PDX mice were generated by engrafting memory CD4+ T cells into NSG mice (NOD/SCID IL2rγ$^{-/-}$, Jax #00557). Memory CD4+ T cells were isolated from peripheral blood mononuclear cells (PBMCs) of a person living with HIV on ART (17). On day 35 post-engraftment, mice received memory CD8+T cells from the same donor and were then intravenously inoculated with 10,000 tissue culture infectious dose 50 (TCID50) of the HIV-1 JRCSF isolate. From day 84, mice were treated subcutaneously with 100 µL of vehicle or a combination ART regimen consisting of TDF (57 mg/kg), FTC (143 mg/kg), and DTG (7 mg/kg) (47), or single PIs (RTV (5.5 mg/kg) and DRV (16.2 mg/kg)) for 8 weeks.

Antiretroviral Drug Dosing. Dosages of ART drugs paralleled those in humans, as documented by both PK/PD data in mice (48) and measurements of antiretroviral drug concentrations in lymph nodes of humanized mice versus humans, showing equivalent tissue levels (49). Notably, our ARTs involved much lower concentrations than those used in many published rodent models of HIV infection (50), where some effects may have been influenced by supra-therapeutic dosing.

Collection and Preparation of Mouse Serum, Plasma, and Platelet Releasate. To obtain serum, whole blood was collected by retrobulbar puncture into tubes without an anticoagulant and incubated at 37°C for 4 h, then centrifuged (13,000*g*, 20 minutes (min), 4°C) to collect the supernatant. To obtain plasma, blood was collected by retrobulbar puncture into a polypropylene tube containing 0.1 volume of 3.8% sodium citrate and PGE_1 (1µM), pH 7.4 and immediately centrifuged at 12,000*g* for 5 min at 4°C. All samples were stored at -80°C until analysis. Washed platelets were prepared as previously described (51). Platelets (0.5×10^9) were stimulated with drug for 10 min at 37°C and releasates were collected as the supernatants following sample centrifugation at 13,000*g* for 15 min at 4°C.

Measurement of TGFβ1 Levels and Signaling. Total TGFβ1 in platelets, serum, and plasma was measured using a DUO-antibody ELISA specific for the activated form of TGFβ1 (R&D Systems) after converting latent TGFβ1 to its active form by acidification followed by neutralization. TGFβ1-induced signaling was measured using a functional bioassay with a the MLEC cell line stably expressing a luciferase reporter gene under the control of the PAI1 promoter (24). Briefly, MLECs (2.5×10^4) were plated in a 96-well tissue culture plate and allowed to adhere for 3 h. The medium was replaced with 90 µL of serum-free DMEM containing antibiotics, and 10 µL of the test sample was added and incubated for 16–18 h at 37°C. PAI1-driven luciferase activity was assayed from cell lysates in an automated luminometer using a luciferase assay system (Promega, Madison, WI). The MLEC assay was used to confirm that active TGFβ1 was driving the signaling response. We also assessed TGFβ1 signaling via Smad activation by stimulating mouse endothelial cells or MLECs with active TGFβ1 and immunoblotting for Smad2/3

phosphorylation using a monoclonal antibody specific for phosphorylated Smad2/3. In some experiments, samples were incubated with a TGFβ1 neutralizing antibody or atorvastatin to assess the specificity of TGFβ1 signaling detected by the PAI1 luciferase and Smad2 phosphorylation assays.

Assessment of Cardiac Function. Systolic and diastolic functions were measured using a high-resolution ultrasound system (Vevo 2100®, VisualSonics) following established methods (51). Systolic function parameters were assessed at end-diastole (d) and end-systole (s) using M-mode images acquired at the level of the papillary muscles in a left parasternal short-axis view. Left ventricular ejection fraction (EF) and fractional shortening (FS) were calculated. Diastolic function indices were recorded in an apical 4-chamber view sound window using pulse-wave or tissue Doppler echocardiography to measure early (E) and late (A) wave peak velocities. A'- and e"- tissue Doppler waves and E/A ratios were calculated following as previously described (51).

Histology: Animals were euthanized, and their hearts were excised, perfused with saline, weighed, and fixed in 4% paraformaldehyde. Myocardial fibrosis was evaluated by staining with hematoxylin and eosin, Masson trichrome, and picrosirius red. The degree of fibrosis was graded on a scale of 0 to 4 by an expert veterinary pathologist unaware of the treatment, using methods established in our lab (51). Masson's trichrome-stained images were acquired at high magnification uaing an Aperio Slide Scanner, and picrosirius red-stained images were acquired using a polarized scanner. An artificial intelligence deep learning method was adapted to develop an algorithm for quantification (52) (Fig. S1).

Oil Red Staining for Cardiac Fat/Lipid. Heart sections were fixed in 4% paraformaldehyde for 24 h, followed by optimal cutting temperature (OCT) mounting and cryo-sectioning at 6 μ thickness. They were stained with Oil-Red O (Millipore), following the manufacturer's protocol. Whole heart sections were scanned using an Aperio Slide Scanner and assembled for quantification using Image scope software.

Immunostaining and Confocal Imaging. Immunofluorescence-stained optimal cutting temperature or paraffin-embedded heart sections (5–6 μ) were brought to room temperature or deparaffinized and washed in phosphate-buffered saline (PBS). Antigens were retrieved in citrate buffer (pH 6.0, Sigma-Aldrich) using a water bath (95°C for 10–12 min) or an antigen retrieval system (Electron Microscopy Science). Heart sections were washed with 0.1% Triton in PBS (PBST), incubated for 1 h in blocking buffer (1% bovine serum albumin in 0.1% PBST), then stained with primary antibody for 2 h at room temperature or overnight at 4°C. Heart sections were then washed three times in PBST, incubated with the secondary antibody in blocking buffer for 1 h, washed again with PBST, and mounted with Fluor G reagent with 4',6-diamidino-2-phenylindole (DAPI). Images were captured with a confocal microscope using 20X or 40X objectives and visualized as 3D projections in Imaris software. For immunohistochemistry, heart tissue sections were deparaffinized/rehydrated, antigens were retrieved using citrate buffer, and non-specific binding was blocked with blocking buffer. Sections were incubated with primary antibodies against perilipin, phosphorylated SMAD2 and SMAD3, PDGFβR, α-SMA, CD31, CD206, PPAR-gamma, and collagen.

Real-time PCR. Total RNA was extracted from cells using the RNeasy Mini Kit (QIAGEN). cDNA was prepared from the RNA using the High-Capacity RNA-to-cDNA Kit (Applied Biosystems), and real-time PCR was performed with ready-made primer sets for

mouse alpha-smooth muscle actin (*ACTA2*) and collagen type 1 alpha 1 (*COL1A1)* on a Bio-Rad real-time PCR system. Thermal cycling conditions: 50°C for 2 min, followed by 95°C for 10 min, 95°C for 15 seconds, and 60°C for 1 min. A total of 40 cycles were run. Data were normalized to the endogenous control gene *GAPDH*.

Statistical analysis. Statistical analysis was performed using GraphPad Prism, SAS version 9.4. Multiple linear regression models were used for fibrosis and diastolic dysfunction. Comparisons were made using the Kruskal-Wallis test, pairwise two-sample Wilcoxon rank sum tests, and two-tailed t-tests. All data are expressed as mean ± standard deviation (SD) and or standard error of the mean (SEM). Differences were considered statistically significant at $P < 0.05$.

Study approval. Mouse experiments were conducted in accordance with the NIH Guide for the Care and Use of Laboratory Animals and were approved in advance by the Institutional Animal Care and Use Committee by Oklahoma Medical Research Foundation and Weill Cornell.

Author contributions: KS, DB, BC, TAA, TV, TW, SG, AD, IGM designed the mouse models of HIV/ART-induced pathology and performed the experiments and collected and analyzed the data. SC analyzed the data and performed statistical modeling. PK, BRJ, KMF, provided essential conceptualization reagents/samples. JL and JA conceived the idea and drafted the manuscript. JA supervised the project, and all authors contributed to the critical revision and final approval of the text.

Funding support: This work was fully supported by HL167656 (JA) and partly supported by HL148123 (JA) and the Angelo Donghia Foundation (JL).

Acknowledgments

We thank P. Dube, T.R. Dilling, and W. Ben for their help with antiretroviral therapy administration, immunoblotting, and tissue harvesting, and M. Deore for reading the manuscript draft. We thank Drs. M. Zanni, T. Neilan, and A. Neilan for their comments and editing of the manuscript. We also thank Life Science Editors for English language editing services.

References

1. Ntsekhe M, and Baker JV. Cardiovascular Disease Among Persons Living With HIV: New Insights Into Pathogenesis and Clinical Manifestations in a Global Context. *Circulation.* 2023;147(1):83-100.
2. Grinspoon SK, Fitch KV, Zanni MV, Fichtenbaum CJ, Umbleja T, Aberg JA, et al. Pitavastatin to Prevent Cardiovascular Disease in HIV Infection. *N Engl J Med.* 2023;389(8):687-99.
3. Lu MT, Ribaudo H, Foldyna B, Zanni MV, Mayrhofer T, Karady J, et al. Effects of Pitavastatin on Coronary Artery Disease and Inflammatory Biomarkers in HIV: Mechanistic Substudy of the REPRIEVE Randomized Clinical Trial. *JAMA Cardiol.* 2024;9(4):323-34.
4. Kolossvary M, Schnittman SR, Zanni MV, Fitch KV, Fichtenbaum CJ, Aberg JA, et al. Pitavastatin, Procollagen Pathways, and Plaque Stabilization in Patients With HIV: A Secondary Analysis of the REPRIEVE Randomized Clinical Trial. *JAMA Cardiol.* 2025;10(3):254-64.
5. Liuize Abramaviciute A, and Mongirdiene A. TGF-beta Isoforms and GDF-15 in the Development and Progression of Atherosclerosis. *Int J Mol Sci.* 2024;25(4).
6. Filip I. Evolving data on heart failure reshape prevention and treatment strategies for people with HIV. *Aids.* 2025;39(11):N15-N6.
7. Zanni MV, Awadalla M, Toribio M, Robinson J, Stone LA, Cagliero D, et al. Immune Correlates of Diffuse Myocardial Fibrosis and Diastolic Dysfunction Among Aging Women With Human Immunodeficiency Virus. *J Infect Dis.* 2019.
8. Thiara DK, Liu CY, Raman F, Mangat S, Purdy JB, Duarte HA, et al. Abnormal Myocardial Function Is Related to Myocardial Steatosis and Diffuse Myocardial Fibrosis in HIV-Infected Adults. *J Infect Dis.* 2015;212(10):1544-51.
9. Shuldiner SR, Wong LY, Peterson TE, Wolfson J, Jermy S, Saad H, et al. Myocardial Fibrosis Among Antiretroviral Therapy-Treated Persons With Human Immunodeficiency Virus in South Africa. *Open Forum Infect Dis.* 2021;8(1):ofaa600.
10. Nelson MD, Szczepaniak LS, LaBounty TM, Szczepaniak E, Li D, Tighiouart M, et al. Cardiac steatosis and left ventricular dysfunction in HIV-infected patients treated with highly active antiretroviral therapy. *JACC Cardiovasc Imaging.* 2014;7(11):1175-7.
11. Janssen-Telders C, Eringa EC, de Groot JR, de Man FS, and Handoko ML. The role of epicardial adipose tissue remodelling in heart failure with preserved ejection fraction. *Cardiovasc Res.* 2025;121(6):860-70.
12. Silverberg MJ, Pimentel N, Leyden WA, Leong TK, Reynolds K, Ambrosy AP, et al. Initial antiretroviral therapy regimen and risk of heart failure. *AIDS.* 2024;38(4):547-56.
13. Neesgaard B, Greenberg L, Miro JM, Grabmeier-Pfistershammer K, Wandeler G, Smith C, et al. Associations between integrase strand-transfer inhibitors and cardiovascular disease in people living with HIV: a multicentre prospective study from the RESPOND cohort consortium. *Lancet HIV.* 2022;9(7):e474-e85.
14. Laurence J, Elhadad S, and Ahamed J. HIV-associated cardiovascular disease: importance of platelet activation and cardiac fibrosis in the setting of specific antiretroviral therapies. *Open Heart.* 2018;5(2):e000823.

15. Alvi RM, Neilan AM, Tariq N, Awadalla M, Afshar M, Banerji D, et al. Protease Inhibitors and Cardiovascular Outcomes in Patients With HIV and Heart Failure. *J Am Coll Cardiol.* 2018;72(5):518-30.
16. Dickie P, Felser J, Eckhaus M, Bryant J, Silver J, Marinos N, et al. HIV-associated nephropathy in transgenic mice expressing HIV-1 genes. *Virology.* 1991;185(1):109-19.
17. McCann CD, van Dorp CH, Danesh A, Ward AR, Dilling TR, Mota TM, et al. A participant-derived xenograft model of HIV enables long-term evaluation of autologous immunotherapies. *J Exp Med.* 2021;218(7).
18. Toribio M, Neilan TG, Awadalla M, Stone LA, Rokicki A, Rivard C, et al. Intramyocardial Triglycerides Among Women With vs Without HIV: Hormonal Correlates and Functional Consequences. *J Clin Endocrinol Metab.* 2019;104(12):6090-100.
19. Neilan TG, Nguyen KL, Zaha VG, Chew KW, Morrison L, Ntusi NAB, et al. Myocardial Steatosis Among Antiretroviral Therapy-Treated People With Human Immunodeficiency Virus Participating in the REPRIEVE Trial. *J Infect Dis.* 2020;222(Suppl 1):S63-S9.
20. Ludbrook SB, Barry ST, Delves CJ, and Horgan CM. The integrin alphavbeta3 is a receptor for the latency-associated peptides of transforming growth factors beta1 and beta3. *Biochem J.* 2003;369(Pt 2):311-8.
21. Ahamed J, Terry H, Choi ME, and Laurence J. Transforming growth factor-beta1-mediated cardiac fibrosis: potential role in HIV and HIV/antiretroviral therapy-linked cardiovascular disease. *AIDS.* 2016;30(4):535-42.
22. Laurence J, Elhadad S, Robison T, Terry H, Varshney R, Woolington S, et al. HIV protease inhibitor-induced cardiac dysfunction and fibrosis is mediated by platelet-derived TGF-beta1 and can be suppressed by exogenous carbon monoxide. *PLoS One.* 2017;12(10):e0187185.
23. Deng Z, Fan T, Xiao C, Tian H, Zheng Y, Li C, et al. TGF-beta signaling in health, disease, and therapeutics. *Signal Transduct Target Ther.* 2024;9(1):61.
24. Abe M, Harpel JG, Metz CN, Nunes I, Loskutoff DJ, and Rifkin DB. An assay for transforming growth factor-beta using cells transfected with a plasminogen activator inhibitor-1 promoter-luciferase construct. *Anal Biochem.* 1994;216(2):276-84.
25. Inia JA, Stokman G, Pieterman EJ, Morrison MC, Menke AL, Verschuren L, et al. Atorvastatin Attenuates Diet-Induced Non-Alcoholic Steatohepatitis in APOE*3-Leiden Mice by Reducing Hepatic Inflammation. *Int J Mol Sci.* 2023;24(9).
26. Araujo FA, Rocha MA, Mendes JB, and Andrade SP. Atorvastatin inhibits inflammatory angiogenesis in mice through down regulation of VEGF, TNF-alpha and TGF-beta1. *Biomed Pharmacother.* 2010;64(1):29-34.
27. Nenna A, Nappi F, Lusini M, Satriano UM, Schiliro D, Spadaccio C, et al. Effect of Statins on Platelet Activation and Function: From Molecular Pathways to Clinical Effects. *Biomed Res Int.* 2021;2021:6661847.
28. Varshney R, Murphy B, Woolington S, Ghafoory S, Chen S, Robison T, et al. Inactivation of platelet-derived TGF-beta1 attenuates aortic stenosis progression in a robust murine model. *Blood Adv.* 2019;3(5):777-88.
29. Holloway CJ, Ntusi N, Suttie J, Mahmod M, Wainwright E, Clutton G, et al. Comprehensive cardiac magnetic resonance imaging and spectroscopy reveal a high burden of myocardial disease in HIV patients. *Circulation.* 2013;128(8):814-22.
30. Oesterle A, Laufs U, and Liao JK. Pleiotropic Effects of Statins on the Cardiovascular System. *Circ Res.* 2017;120(1):229-43.

31. deFilippi C, Christenson R, Joyce J, Park EA, Wu A, Fitch KV, et al. Brief Report: Statin Effects on Myocardial Fibrosis Markers in People Living With HIV. *J Acquir Immune Defic Syndr.* 2018;78(1):105-10.
32. Pirillo A, and Catapano AL. Pitavastatin and HDL: Effects on plasma levels and function(s). *Atherosclerosis Supp.* 2017;27:E1-E9.
33. Lo J, Lu MT, Ihenachor EJ, Wei J, Looby SE, Fitch KV, et al. Effects of statin therapy on coronary artery plaque volume and high-risk plaque morphology in HIV-infected patients with subclinical atherosclerosis: a randomised, double-blind, placebo-controlled trial. *Lancet HIV.* 2015;2(2):e52-63.
34. Elahi S, Weiss RH, and Merani S. Atorvastatin restricts HIV replication in CD4+ T cells by upregulation of p21. *AIDS.* 2016;30(2):171-83.
35. Wiggins BS, Lamprecht DG, Jr., Page RL, 2nd, and Saseen JJ. Recommendations for Managing Drug-Drug Interactions with Statins and HIV Medications. *Am J Cardiovasc Drugs.* 2017;17(5):375-89.
36. Marunouchi T, Matsumura K, Fuji E, Iwamoto A, and Tanonaka K. Simvastatin Attenuates Cardiac Fibrosis under Pathophysiological Conditions of Heart Failure with Preserved Left Ventricular Ejection Fraction by Inhibiting TGF-beta Signaling. *Pharmacology.* 2024;109(1):43-51.
37. Du Y, Xiao H, Wan J, Wang X, Li T, Zheng S, et al. Atorvastatin attenuates TGF-beta1-induced fibrogenesis by inhibiting Smad3 and MAPK signaling in human ventricular fibroblasts. *Int J Mol Med.* 2020;46(2):633-40.
38. Walpert AR, Gupta M, Dunderdale CN, Haptu HH, Manandhar M, deFilippi CR, et al. Exploring the PREVENT HF score and myocardial function among persons with HIV. *AIDS.* 2025.
39. Foldyna B, Mayrhofer T, Zanni MV, Lyass A, Barve R, Karady J, et al. Pericoronary Adipose Tissue Density, Inflammation, and Subclinical Coronary Artery Disease Among People With HIV in the REPRIEVE Cohort. *Clin Infect Dis.* 2023;77(12):1676-86.
40. Toribio M, Park MH, Zanni MV, Robbins GK, Burdo TH, Williams KC, et al. HDL Cholesterol Efflux Capacity in Newly Diagnosed HIV and Effects of Antiretroviral Therapy. *J Clin Endocrinol Metab.* 2017;102(11):4250-9.
41. Toribio M, Neilan TG, and Zanni MV. Heart Failure among People with HIV: Evolving Risks, Mechanisms, and Preventive Considerations. *Curr HIV/AIDS Rep.* 2019;16(5):371-80.
42. Capeau J, Lagathu C, Ngono Ayissi K, Feve B, and Bereziat V. HIV and adipose tissue: A long history linked to therapeutic classes of antiretrovirals. *Ann Endocrinol (Paris).* 2024;85(3):255-8.
43. Talathi R, Anekwe CV, and Toribio M. Epidemiology of obesity among people with HIV. *Curr Opin HIV AIDS.* 2024;19(1):1-5.
44. Hayat J, Shah NP, Agarwala A, Khan MS, and Butler J. GLP-1 Receptor Agonists and Cardiovascular Disease: What Do Clinicians Need to Know? *Curr Atheroscler Rep.* 2024;26(8):341-51.
45. Lake JE, Kitch DW, Kantor A, Muthupillai R, Klingman KL, Vernon C, et al. The Effect of Open-Label Semaglutide on Metabolic Dysfunction-Associated Steatotic Liver Disease in People With HIV. *Ann Intern Med.* 2024;177(6):835-8.
46. Herbertz S, Sawyer JS, Stauber AJ, Gueorguieva I, Driscoll KE, Estrem ST, et al. Clinical development of galunisertib (LY2157299 monohydrate), a small molecule inhibitor of

transforming growth factor-beta signaling pathway. *Drug Des Devel Ther.* 2015;9:4479-99.
47. Whitney JB, Lim SY, Osuna CE, Kublin JL, Chen E, Yoon G, et al. Prevention of SIVmac251 reservoir seeding in rhesus monkeys by early antiretroviral therapy. *Nat Commun.* 2018;9(1):5429.
48. Labarthe L, Gele T, Gouget H, Benzemrane MS, Le Calvez P, Legrand N, et al. Pharmacokinetics and tissue distribution of tenofovir, emtricitabine and dolutegravir in mice. *J Antimicrob Chemother.* 2022;77(4):1094-101.
49. Burgunder E, Fallon JK, White N, Schauer AP, Sykes C, Remling-Mulder L, et al. Antiretroviral Drug Concentrations in Lymph Nodes: A Cross-Species Comparison of the Effect of Drug Transporter Expression, Viral Infection, and Sex in Humanized Mice, Nonhuman Primates, and Humans. *J Pharmacol Exp Ther.* 2019;370(3):360-8.
50. Mak IT, Chmielinska JJ, Spurney CF, Weglicki WB, and Kramer JH. Combination ART-Induced Oxidative/Nitrosative Stress, Neurogenic Inflammation and Cardiac Dysfunction in HIV-1 Transgenic (Tg) Rats: Protection by Mg. *Int J Mol Sci.* 2018;19(8).
51. Meyer A, Wang W, Qu J, Croft L, Degen JL, Coller BS, et al. Platelet TGF-beta1 contributions to plasma TGF-beta1, cardiac fibrosis, and systolic dysfunction in a mouse model of pressure overload. *Blood.* 2012;119(4):1064-74.
52. Fu X, Liu T, Xiong Z, Smaill BH, Stiles MK, and Zhao J. Segmentation of histological images and fibrosis identification with a convolutional neural network. *Comput Biol Med.* 2018;98:147-58.

Figure 1

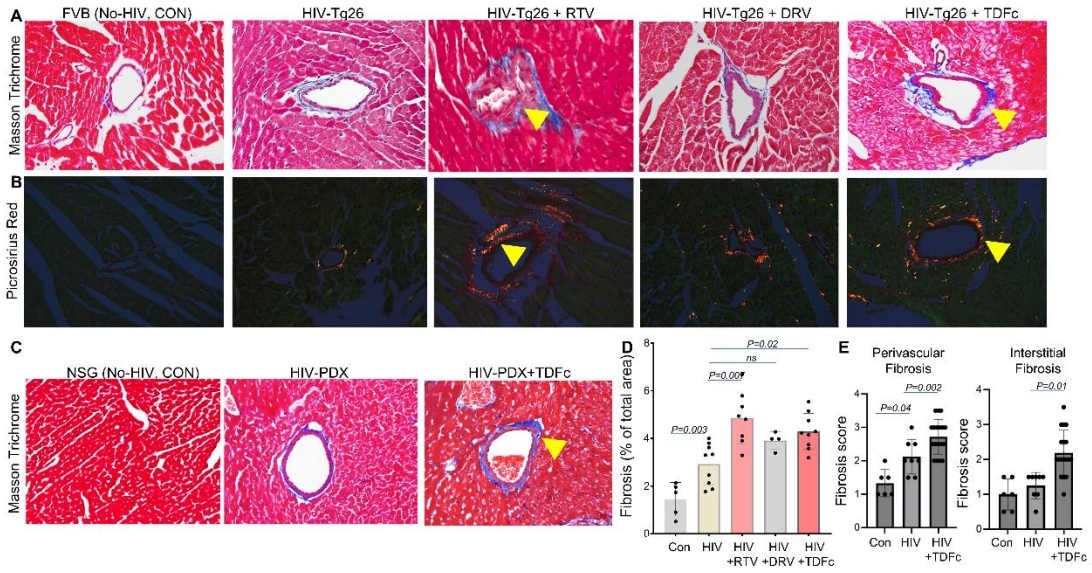

Figure 1. Effect of ART on cardiac fibrosis in HIV mice. (**A**) Representative images of Masson trichome staining of heart sections from FVB-No HIV controls, HIV-Tg26 mice, and HIV-Tg26 mice treated with antiretroviral therapy (ART) ritonavir (RTV), darunavir (DRV), or the tenofovir-

emtricitabine-dolutegravir (TDF-FTC-DTG) cocktail (TDFc) for eight weeks. Excessive collagen is indicated in blue. (**B**) Representative images of picrosirius red staining, showing fibrotic areas as a mixture of green, red, and yellow, under polarized light microscopy. (**C**) Representative images of Masson trichome staining of heart sections from NSG-controls, HIV-infected (HIV-PDX) mice, and HIV-PDX mice treated with the TDF-FTC-DTG cocktail for eight weeks. (**D**) Quantification of fibrotic areas in Masson trichome and picrosirius red images showed that HIV-infected mice had higher cardiac fibrosis than controls. ART-treated HIV-Tg26 mice, with the exception of those treated with DRV, had more fibrotic areas than untreated ones. (**E**) Blind scoring for fibrosis by microscopy on a 0–4 scale showed that ART-treated mice exhibited higher perivascular and interstitial fibrosis than untreated HIV-PDX control mice. Both patterns of fibrosis were quantified from whole-heart Masson trichome and picrosirius red images acquired from a slide scanner (Supplementary Figures S1A–C). In **(D)** and **(E)**, total, perivascular, and interstitial fibrosis were quantified using the algorithm shown in Fig. S1A, or blindly by a pathologist and a trained technician who were unaware of mouse genotype. Each dot in the bar graphs represents individual mouse; data are presented as Mean ± SD; p values <0.05 considered significant using standard Student t-test.

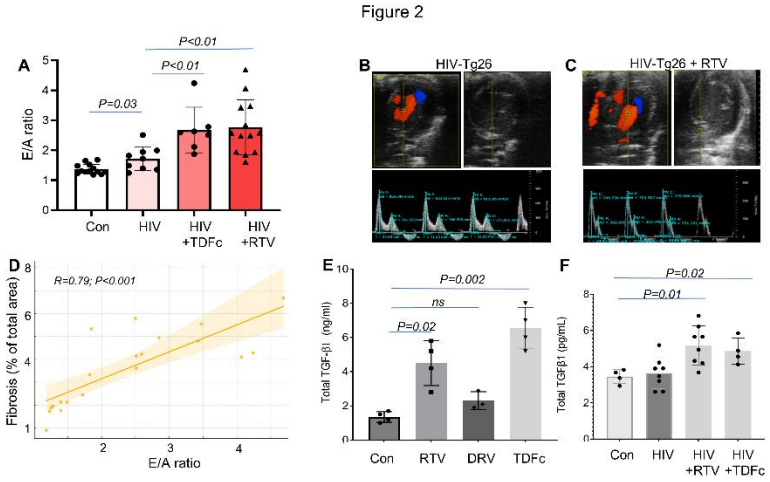

Figure 2. Effect of ART on cardiac function in HIV-Tg26 mice. (**A**) Boxplot showing increased early-to-late (E/A) ventricular filling velocity ratios indicating impaired diastolic function following eight weeks of exposure to RTV or the TDF-FTC-DTG cocktail (TDFc) compared with untreated HIV-Tg26 control mice. (**B**, **C**) Representative ultrasound images (Vevo2100) showing 4-chamber views with color-Doppler (upper left; blood flow in red) across the mitral valve annulus (upper right) and power-Doppler (lower panels; peak E and A wave velocities) in HIV mice without (**B**) or with (**C**) RTV treatment for eight weeks. (**D**) E/A ratios directly correlated with cardiac fibrosis in control

and ART-treated HIV mice. (**E**, **F**) Barplots showing total TGFβ1 levels as measured by ELISA in (**E**) platelet releasates (10^9 per mL) prepared from healthy human volunteers–before and after stimulation with RTV (5 μM), darunavir (DRV; 15 μM), or TDFc. (**F**) plasma prepared from HIV-Tg26 mice treated with RTV or TDFc. Each dot in the bar graphs represents individual mouse; data are presented as Mean ± SD; p values <0.05 considered significant using standard Student t-test.

Figure 3

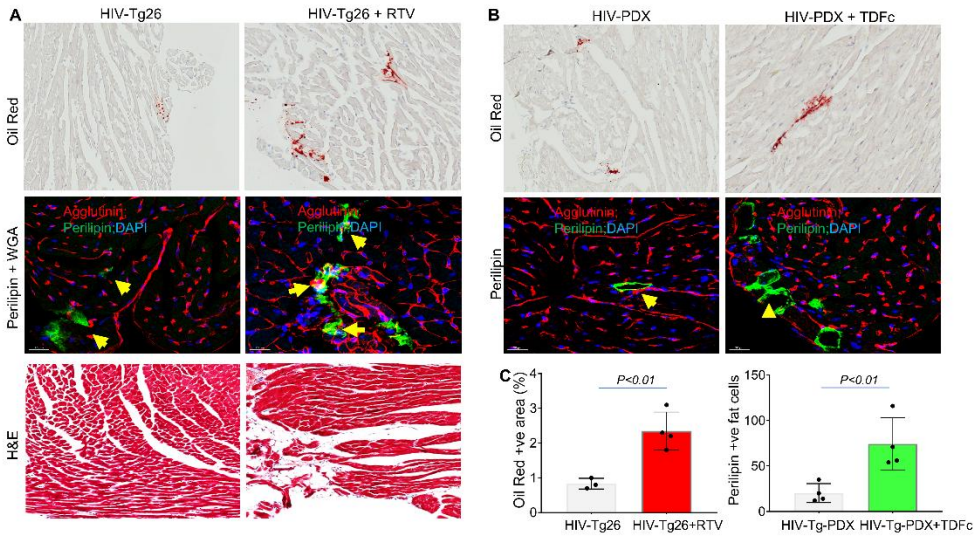

Figure 3. ART-induced ectopic fat deposition in the heart is associated with cardiac fibrosis in HIV-Tg26 and HIV-PDX mice. (**A-B**) HIV-Tg26 and HIV-PDX mice were challenged with RTV (left) or TDF-FTC-DTG (right). Oil-Red O-positive areas indicate lipid/fat cell deposition in the heart (upper panels), which were confirmed by perilipin immunofluorescence with confocal microscopy (middle panels) and by H&E staining (A, lower panels). Oil-Red O-positive areas were also matched with fibrotic areas. (**C**) Quantification of lipid (**left**) or fat cells (**right**) from Oil-Red O-positive or perilipin-positive regions, respectively in the hearts of ART-treated HIV-Tg26 and HIV-PDX mice.

Each dot in the bar graphs represents individual mouse; data are presented as Mean ± SD; p values <0.05 considered significant using standard Student t-test.

Figure 4

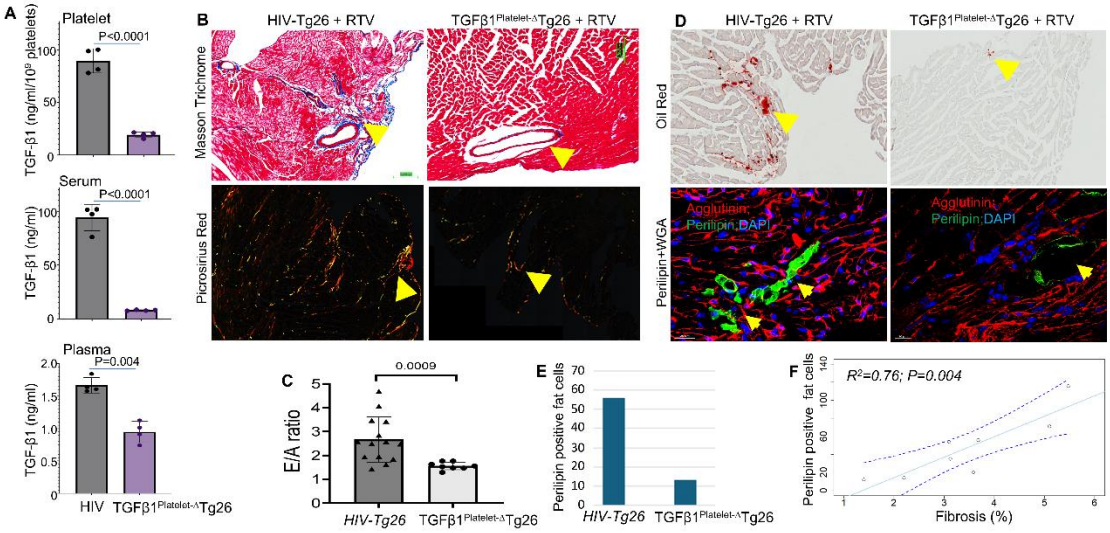

Figure 4. *TGFβ1*$^{Platelet\text{-}\Delta}$*Tg26* mice are partially protected from developing RTV-induced cardiac fibrosis and deterioration of diastolic function. (**A**) TGFβ1$^{Platelet\text{-}\Delta}$Tg26 mice (purple) showed a >90% decrease in TGFβ1 in platelets and serum, and a >50% decrease in plasma TGFβ1, compared with littermate control HIV-Tg26 mice (gray), as measured by ELISA (n = 4). (**B**) Images of heart sections from RTV-challenged HIV-Tg26 or TGFβ1$^{Platelet\text{-}\Delta}$Tg26 mice were captured under polarized light, revealing fibrotic areas in blue in Masson trichrome staining, and as mixtures of green, red, and yellow in picrosirius red staining. TGFβ1$^{Platelet\text{-}\Delta}$Tg26 mice accumulated lower collagen levels than HIV-Tg26 mice, as confirmed by quantification of picrosirius red staining, which revealed smaller fibrotic areas in TGFβ1$^{Platelet\text{-}\Delta}$Tg26 mice (2.5% ± 0.5%) compared with HIV-Tg26 mice (3.3% ± 0.7%; *P* <0.01 by Student t-test). (**C**) E/A ratios measured by echocardiography, showing protection from impairment of diastolic dysfunction in TGFβ1$^{Platelet\text{-}\Delta}$Tg26 mice (light gray). (**D**) Oil-Red O and perilipin staining show reduced fat cell accumulation in heart tissue from RTV-challenged TGFβ1$^{Platelet\text{-}\Delta}$Tg26 mice compared with RTV-challenged HIV-Tg26 mice. (**E**) Barplot showing the number of perilipin-positive fat cells per heart in RTV-challenged TGFβ1$^{Platelet\text{-}\Delta}$Tg26 and HIV-*Tg26* mice, quantified from confocal microscopy images. Each bar represents the average of two heart sections). (**F**) Correlation plot showing the positive association between cardiac fibrosis

and fat cell deposition in the hearts of HIV-Tg26 mice and *TGFβ1*$^{Platelet\text{-}\Delta}$*Tg26* mice challenged with RTV.

Figure 5

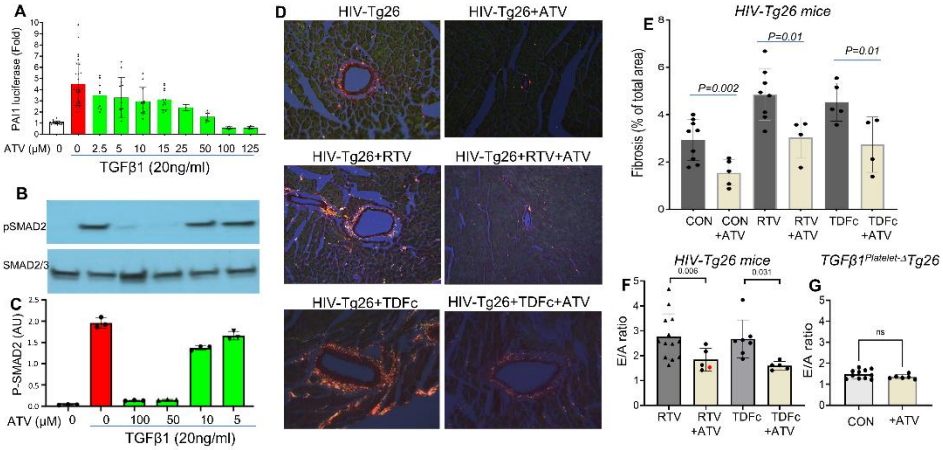

Figure 5. Atorvastatin suppresses TGFβ1 signaling, cardiac fibrosis, and fat cell deposition and improves diastolic dysfunction in HIV mice. (**A**) Atorvastatin (ATV) inhibited TGFβ1-mediated PAI1 luciferase activity and (**B**) SMAD2 phosphorylation in a dose-dependent manner in mink lung epithelial cells stimulated with platelet TGFβ1 (20ng/ml) for 16–18h. (**C**) Quantification of dose-dependent inhibition of SMAD2 phosphorylation levels by ATV. (**D**) Picrosirius red staining of heart sections from HIV-Tg26 mice challenged with vehicle, ATV, RTV, or the TDF-FTC-DTG cocktail (TDFc) for eight weeks, showing that ATV halted cardiac fibrosis, as visualized under polarized light. (**E**) Quantification of picrosirius red staining showing significantly lower fibrosis in ATV-co-treated mice compared with mice exposed to vehicle, RTV, or TDFc alone. Group comparisons were performed using the Wilcoxon rank-sum test. (**F**) E/A ratios measured by echocardiography, showing lower impairment of diastolic function in HIV-Tg26 mice co-treated with ATV (yellow) compared with those exposed to RTV or TDFc alone. (**G**) Barplot showing no significant difference in diastolic functions (as measured by E/A ratio) in combined PF4Cre- (n=3) and G1bCre-(n=3)Tgfb1$^{flox/flox}$ (TGFβ1$^{Platelet\text{-}\Delta}$Tg26) mice treated with ATV for eight weeks (light gray). Each dot represents Masson trichome or picrosirius red quantifications from whole heart

images from individual mouse (Fig. S1A-C); data are presented as Mean ± SD; p values <0.05 considered significant using standard Student t-test.

Figure 6

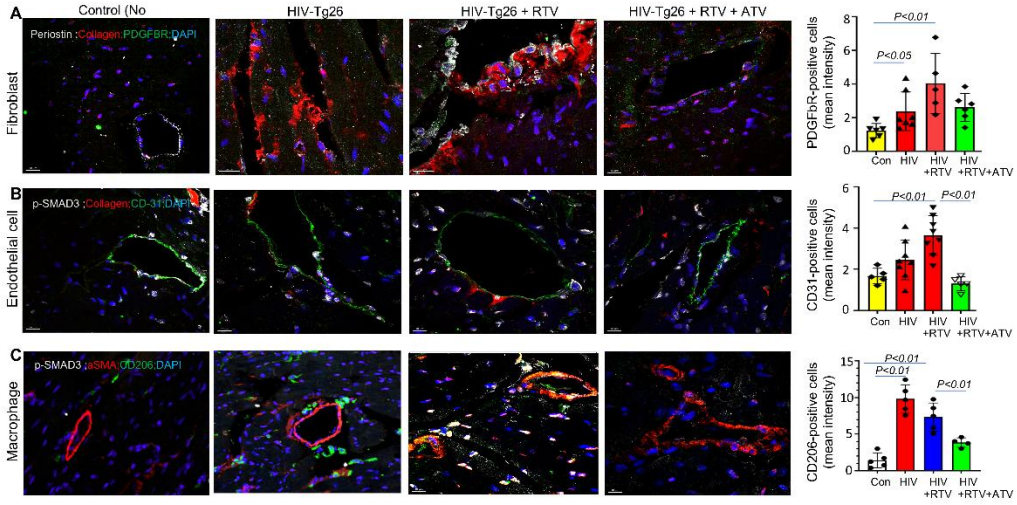

Figure 6. Atorvastatin inhibits Smad signaling and mesenchymal transition in the hearts of HIV-Tg26 mice. Confocal microscopy images and immunofluorescence quantification of myofibroblast markers PDGFβR (fibroblasts) (**A**), CD31 (endothelial cells) (**B**), and CD206 (macrophages) (**C**) in the hearts of HIV-negative control mice, untreated and RTV-treated HIV-Tg26 mice, and atorvastatin + RTV-cotreated HIV-Tg26 mice. Each dot in the bar graphs

represents individual mouse; data are presented as Mean ± SD; p values <0.05 considered significant using standard Student t-test.

Figure 7

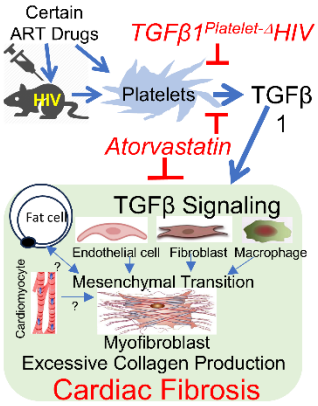

Figure 7. Graphic model showing that HIV-ART induces the release of TGFβ1 from platelets, which activates downstream TGFβ signaling in various cardiac cell types. This drives the mesenchymal transition of these cardiac cells into myofibroblasts, which produce excessive collagen and leads to cardiac fibrosis. These responses can be mitigated by atorvastatin administration, which inhibits TGFβ signaling and platelet activation.

Table 1. Hematologic values in control and transgenic HIV mice

Genotype	WBC *K/μL*	*NE K/μL*	*LY K/μL*	*MO K/μL*	*EO K/μL*	*RBC M/μL*	*HB g/dL*	*HCT %*	*PLT K/μL*	*MPV fL*	*NE/LY*
Control mice without HIV (n=12)	6.73±1.87	0.80±0.38	5.36±1.43	0.54±0.25	0.02±0.04	9.20±0.80	12.67±1.01	54.29±4.60	1176.67±315.80	4.08±0.21	0.15±0.07
Tg26 (n=18)	9.79±6.18	2.17±1.71	6.48±4.11	1.08±0.72	0.05±0.07	6.88±1.94	9.47±2.59	39.69±13.84	993.89±226.78	4.31±0.19	0.34±0.21
Tg26 + (RTV) (n=13)	8.08±5.59	2.14±2.29	5.14±3.08	0.72±0.50	0.03±0.06	8.41±1.56	10.12±1.73	46.42±8.90	1251.92±160.35	4.20±0.26	0.40±0.22
TGFβ1$^{Platelet\ \Delta}$Tg26 (n=6)	7.60±2.34	0.97±0.39	6.18±1.86	0.40±0.10	0.05±0.05	9.20±0.48	10.50±0.50	44.50±2.65	930.00±108.97	4.07±0.15	0.16±0.03
Tg26 + (TDF) (n=6)	10.97±5.03	3.07±2.15	7.02±2.92	0.87±0.25	0.02±0.03	7.65±1.11	10.50±1.95	43.50±6.56	1214.17±228.11	4.12±0.29	10.97±0.18
Tg26 + Atorvastatin (n=7)	10.40±5.00	1.36±0.91	7.38±3.49	1.62±1.05	0.02±0.03	7.63±1.37	10.64±1.97	45.71±10.11	838.57±355.62	4.64±1.17	0.19±0.11

WBC=white blood cells; RBC=red blood cells; Hb=hemoglobin; HCT=hematocrit; PLT=platelets; MPV=mean platelet volume; NE=neutrophils; LY=lymphocytes; MO=monocytes; EO=eosinophils; K=1000; M=million.